Translational Oncology
www.transonc.com

Volume 11 Number 5 October 2018 pp. 1128–1136 1128

Diffusion-Weighted MRI Is Insensitive to Changes in the Tumor Microenvironment Induced by Antiangiogenic Therapy[1,2]

Anette Hauge, Catherine S. Wegner, Jon-Vidar Gaustad, Trude G. Simonsen, Lise Mari K. Andersen and Einar K. Rofstad

Group of Radiation Biology and Tumor Physiology, Department of Radiation Biology, Institute for Cancer Research, Oslo University Hospital, Oslo, Norway

Abstract

Antiangiogenic treatment (AAT) used in combination with radiation therapy or chemotherapy is a promising strategy for the treatment of several cancer diseases. The vascularity and oxygenation of tumors may be changed significantly by AAT, and consequently, a noninvasive method for monitoring AAT-induced changes in these microenvironmental parameters is needed. The purpose of this study was to evaluate the potential usefulness of diffusion-weighted magnetic resonance imaging (DW-MRI). DW-MRI was conducted with a Bruker Biospec 7.05-T scanner using four diffusion weightings and diffusion sensitization gradients in three orthogonal directions. Maps of the apparent diffusion coefficient (ADC) were calculated by using a monoexponential diffusion model. Two cervical carcinoma xenograft models (BK-12, HL-16) were treated with bevacizumab, and two pancreatic carcinoma xenograft models (BxPC-3, Panc-1) were treated with sunitinib. Pimonidazole and CD31 were used as markers of hypoxia and blood vessels, respectively, and fraction of hypoxic tissue (HF_{Pim}) and microvascular density (MVD) were quantified by analyzing immunohistochemical preparations. MVD decreased significantly after AAT in BK-12, HL-16, and BxPC-3 tumors, and this decrease was sufficiently large to cause a significant increase in HF_{Pim} in BK-12 and BxPC-3 tumors. The ADC maps of treated tumors and untreated control tumors were not significantly different in any of these three tumor models, suggesting that the AAT-induced microenvironmental changes were not detectable by DW-MRI. DW-MRI is insensitive to changes in tumor vascularity and oxygenation induced by bevacizumab or sunitinib treatment.

Translational Oncology (2018) 11, 1128–1136

Introduction

Macroscopic tumor growth is in most cases angiogenesis dependent, and several molecular pathways promoting tumor angiogenesis have been identified, including the vascular endothelial growth factor (VEGF) pathway [1]. Antiangiogenic treatment (AAT) is a promising therapeutic modality for cancer, and many antiangiogenic agents targeting the VEGF pathway have been identified, including bevacizumab and sunitinib [2]. Clinical investigations have revealed that the potential of AAT is limited when used as a single therapeutic modality, but the therapeutic benefit may be significant when AAT is used in combination with conventional chemotherapy or radiation therapy [3].

Preclinical studies have revealed that AAT may cause significant vessel pruning and increased hypoxia in some tumors and vessel normalization, increased blood flow, and reduced fraction of hypoxic tissue in others [4,5]. Improved oxygenation may enhance the antitumor effects of radiation therapy and some chemotherapeutic agents, whereas increased hypoxia may impair the effects of most

Address all correspondence to: Einar K. Rofstad, PhD, Department of Radiation Biology, Institute for Cancer Research, Oslo University Hospital, Box 4953 Nydalen, 0424 Oslo, Norway. E-mail: einar.k.rofstad@rr-research.no

[1] Funding: This work was supported by the Norwegian Cancer Society and the South-Eastern Norway Regional Health Authority.

[2] Conflict of Interest: The authors have no conflicts of interest.

Received 30 May 2018; Revised 3 July 2018; Accepted 6 July 2018

1936-5233/18

https://doi.org/10.1016/j.tranon.2018.07.005

treatment modalities and promote the development of regional and distant metastases [6]. The influence of AAT on the vascular network and oxygenation of tumors may depend on the angiogenic profile and microvascular architecture of the tumor tissue as well as time after treatment and the AAT protocol, including antiangiogenic agent and drug dose [7,8].

AAT used prior to or concurrent with chemotherapy or radiation therapy cannot be expected to be beneficial if the AAT has detrimental effects on tumor vascularization and oxygenation. A noninvasive method is therefore needed to monitor the effects of AAT on the tumor microenvironment, and it has been suggested that diffusion-weighted magnetic resonance imaging (DW-MRI) would be useful for that purpose [9,10]. DW-MRI is a well-established and commonly used imaging modality in the diagnostics of cancer, and in most clinical studies, parametric images of the apparent diffusion coefficient (ADC) are used to visualize and quantify DW-MRI data [11]. The ADC is sensitive to the Brownian motion of water molecules, which is restricted by cell membranes, extracellular matrix, and other extracellular tissue components [12].

AAT-induced changes in the ADC of tumors have been examined in several clinical studies, and unfortunately, these studies have provided conflicting observations [11]. Some studies report increased ADC values after AAT, whereas other studies suggest that AAT may induce a decrease in ADC, and moreover, most of these studies do not provide a biological explanation of the observed change in ADC [9–12]. Most likely, detailed preclinical studies are needed to reveal whether ADC is sensitive to changes in the tumor microenvironment induced by AAT.

The purpose of the study reported here was to investigate whether the ADC of tumors given AAT differs from that of untreated tumors and, hence, whether DW-MRI is a potentially useful imaging modality for monitoring AAT-induced changes in the tumor microenvironment. Tumors of two patient-derived xenograft models of squamous cell carcinoma of the uterine cervix (BK-12 and HL-16) and two cell line–derived xenograft models of pancreatic ductal adenocarcinoma (BxPC-3 and Panc-1) were included in the study. These models were selected for the study because they were expected to differ significantly in ADC due to highly different tumor histology. AAT was given by using bevacizumab and sunitinib as antiangiogenic agents. Bevacizumab is a humanized monoclonal antibody that binds to all isoforms of VEGF-A, and this antibody is approved by the US Food and Drug Administration (FDA) for the treatment of several

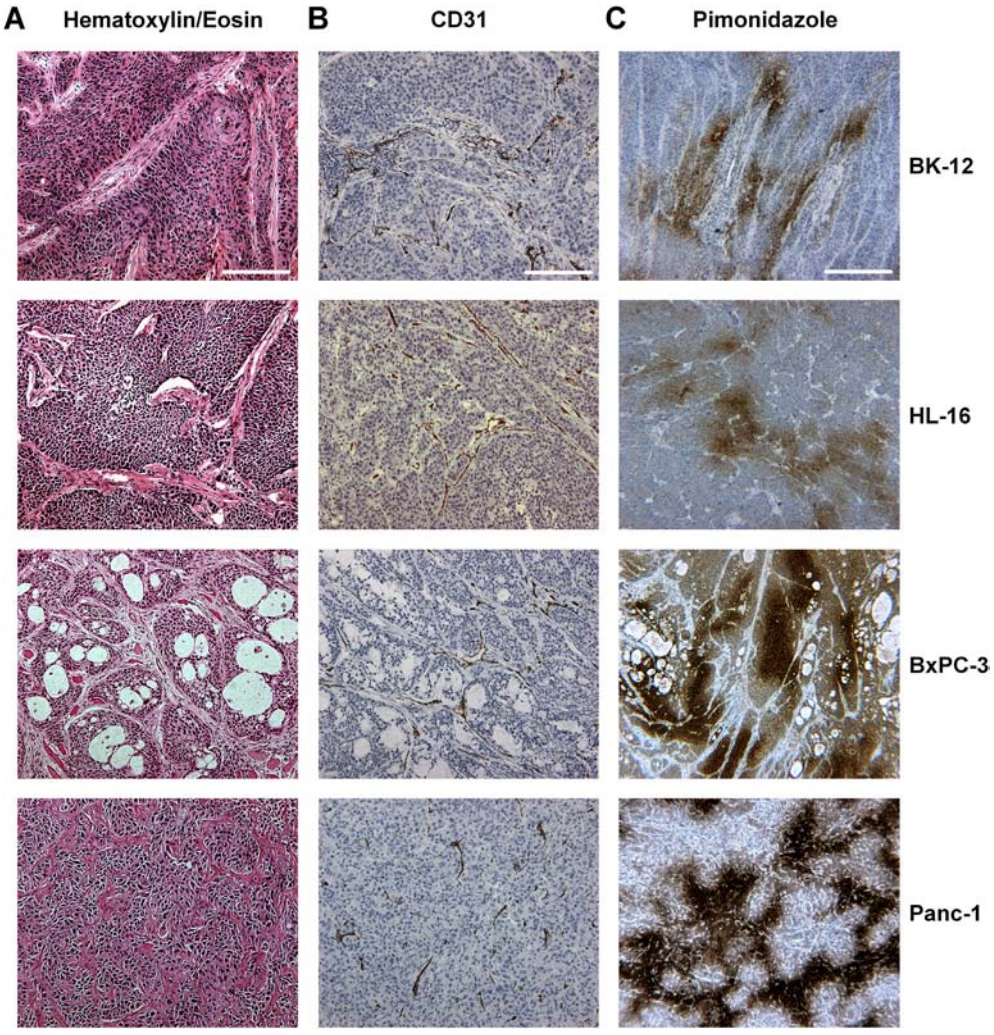

Figure 1. Tumor histology. Representative histological preparations of BK-12, HL-16, BxPC-3, and Panc-1 tumors stained with hematoxylin and eosin (A), immunostained for CD31 to visualize blood vessels (B), or immunostained for pimonidazole to visualize hypoxic tissue (C). Scale bars, 200 μm in A and B and 500 μm in C.

cancer diseases [13]. Sunitinib is an FDA-approved tyrosine kinase inhibitor that targets VEGF receptors 1-3, platelet-derived growth factor receptors α and β, fms-like tyrosine kinase receptor-3, and stem cell growth factor receptor [14].

Materials and Methods

Tumor Models

BK-12 and HL-16 cervical carcinomas and BxPC-3 and Panc-1 pancreatic carcinomas grown in adult (8-12 weeks of age) female BALB/c *nu/nu* mice were used as preclinical tumor models. The cervical carcinoma models were established in our laboratory [15], whereas the pancreatic carcinoma models were purchased from the American Type Culture Collection, VA, USA. BK-12 and HL-16 tumors in passage 4 or 5 were used in this study, and the tumors were initiated from our frozen stock (passage 2) as described earlier [15]. BxPC-3 and Panc-1 tumors were initiated from cells cultured in RPMI-1640 (25 mmol/l HEPES and L-glutamine) medium supplemented with 13% bovine calf serum, 250 mg/l penicillin, and 50 mg/l streptomycin [16]. Approximately 5.0×10^5 BK-12 or HL-16 cells or ~2.5×10^6 BxPC-3 or Panc-1 cells suspended in 10-30 μl of Hanks' balanced salt solution were inoculated in the left *quadriceps femoris* to initiate tumor growth. The animal experiments were approved by the Norwegian National Animal Research Authority and were conducted in accordance with the Interdisciplinary Principles and Guidelines for the use of Animals in Research, Marketing, and Education (New York Academy of Sciences, New York, NY, USA).

Antiangiogenic Treatment

Bevacizumab (Avastin; Hoffman-La Roche, Basel, Switzerland) was dissolved in physiological saline and administered by intraperitoneal injection. The injection volume varied with the mouse weight and was 0.25 ml for a 25-g mouse. Tumor-bearing mice were treated with 3 bevacizumab doses of 10 mg/kg or vehicle over a period of 8 days.

Sunitinib L-malate (LC Laboratories, Woburn, MA, USA) was dissolved in hydrochloric acid (1.0 molar ratio of sunitinib). Polysorbate 80 (0.5%; Sigma-Aldrich, Schnelldorf, Germany), polyethylene glycol 300 (10%; Sigma Aldrich), sodium hydroxide to adjust to a pH of 3.5, and sterile water were added to the solution. Tumor-bearing mice were treated with 4 sunitinib doses of 40 mg/kg or vehicle over a period 4 days. Sunitinib and vehicle were administered orally in volumes of ~0.2 ml by using a gavage.

Treatment effects were evaluated by DW-MRI and/or immunohistochemistry. The DW-MRI was conducted 3 days after the last bevacizumab dose or 1 day after the last sunitinib dose, and the tumors were resected for immunohistochemical examinations shortly after the DW-MRI.

Magnetic Resonance Imaging

MRI was carried out using a Bruker Biospec 7.05-T bore magnet and a mouse quadrature volume coil (Bruker Biospin, Ettlingen, Germany). The tumors were positioned in the isocenter of the magnet and imaged with axial slices covering the entire volume. The mice were given gas anesthesia (~4.0% Sevofluran in O_2; Baxter, IL, USA) at a flow rate of 0.5 l/min during imaging. Respiration rate and body core temperature were monitored continuously by using an abdominal pressure sensitive probe and a rectal temperature probe (Small Animal Instruments, New York, NY, USA). The body core temperature was kept at 37°C by automated hot air flow regulation, and the gas anesthesia was adjusted manually to maintain a stable respiration rate. Anatomical T_2-weighted images were obtained prior to DW-MRI by using a fast spin echo pulse sequence (RARE) with a repetition time (TR) of 2500 milliseconds, an echo time (TE) of 35 milliseconds, an image matrix of 128 × 128, a field of view (FOV) of 3

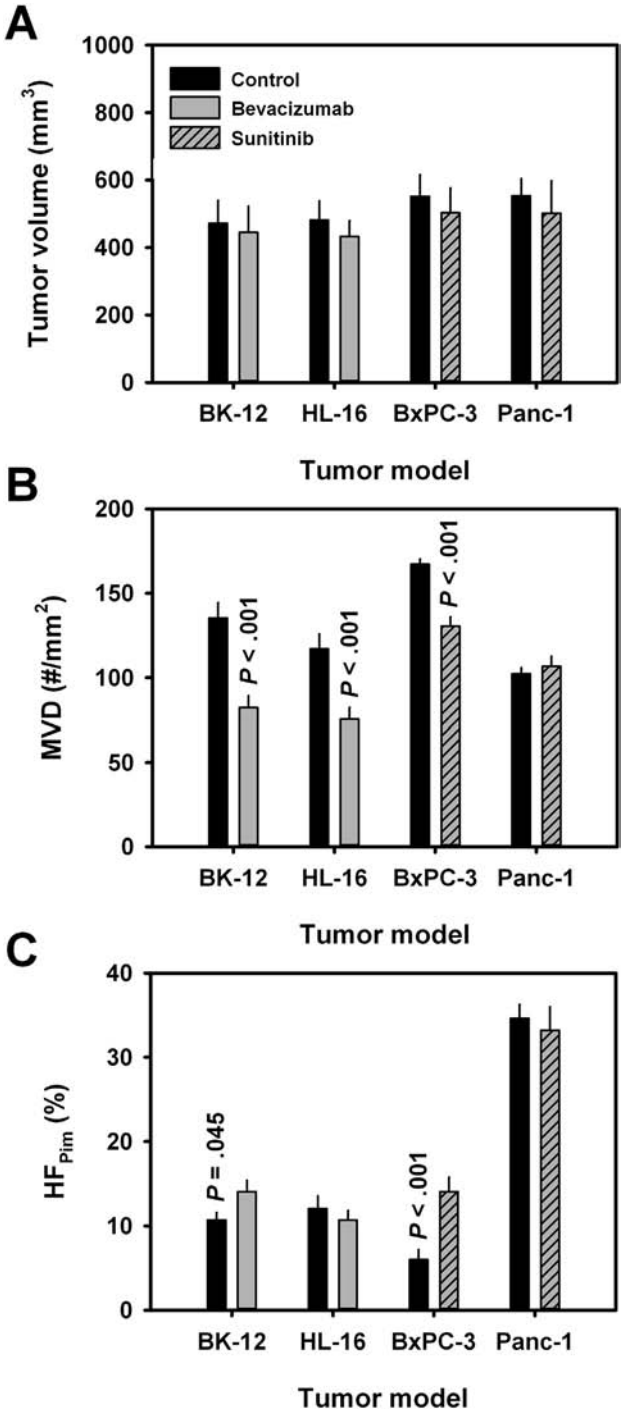

Figure 2. MVD and HF_{Pim} in untreated and treated tumors. Untreated control tumors and treated tumors of the same size (A) are compared with respect to MVD (B) and HF_{Pim} (C). BK-12 and HL-16 tumors were treated with bevacizumab, and BxPC-3 and Panc-1 tumors were treated with sunitinib. Columns and bars, mean ± standard error (n = 7-19).

× 3 cm^2, a slice thickness of 0.7 mm, a slice gap of 0.3 mm, 2 averages, and fat suppression.

DW-MRI was conducted by using a diffusion-weighted single-shot fast spin echo pulse sequence (RARE) with a TR of 1300 milliseconds, a TE of 26 milliseconds, an image matrix of 64 × 64, a FOV of 3 × 3 cm^2, a slice thickness of 0.7 mm, and a slice gap of 0.3 mm [17]. Four diffusion weightings with diffusion encoding constants (b) of 200, 400, 700, and 1000 s/mm^2, a diffusion gradient duration of 7 milliseconds, and a diffusion gradient separation time of 14 milliseconds were used. Diffusion sensitization gradients were applied in three orthogonal directions, and ADC values were calculated for each direction by using a monoexponential diffusion model and in-house-made software developed in Matlab (MathWorks, Natick, MA, USA). Finally, the directional diffusion images were averaged on a voxel-by-voxel basis to nondirectional diffusion images, and these nondirectional images were used to calculate ADC maps.

The analysis of the DW-MRI data was based on the entire volume of the tumors without including peritumoral muscle tissue. Regions of interest (ROIs) encompassing the tumor tissue were depicted in the T_2-weighted anatomical images acquired prior to the DW-MRI, and these ROIs were transferred to the DW images, as illustrated and described in detail elsewhere [16]. Moreover, it was verified that the tumors did not move during imaging [16], and consequently, motion correction algorithms were not used.

Immunohistochemistry

Histological sections were stained with hematoxylin and eosin or immunostained for blood vessels or hypoxia. Pimonidazole [1-[(2-hydroxy-3-piperidinyl)-propyl]-2-nitroimidazole] was administered as described elsewhere and used as a marker of tumor hypoxia [18]. An anti-pimonidazole rabbit polyclonal antibody (Professor James A. Raleigh, University of North Carolina, Chapel Hill, NC, USA) or an anti-mouse CD31 rabbit polyclonal antibody (Abcam, Cambridge, UK) was used as primary antibody. Diaminobenzidine was used as chromogen, and hematoxylin was used for counterstaining. Quantitative studies were carried out on preparations cut through the central regions of tumors, and three randomly selected sections of each staining were analyzed for each tumor. Blood vessel density was scored by counting CD31-positive vessels in whole tumor cross-sections as described elsewhere [19]. Fraction of pimonidazole-positive tissue (i.e., hypoxic fraction) was defined as the area fraction of non-necrotic tissue showing positive staining and assessed by image analysis [20].

Statistical Analysis

The Spearman rank order correlation test was used to search for correlations between parameters. Comparisons of data were conducted by using the Student t test (single comparisons) or by one-way ANOVA followed by the Bonferroni test (multiple comparisons)

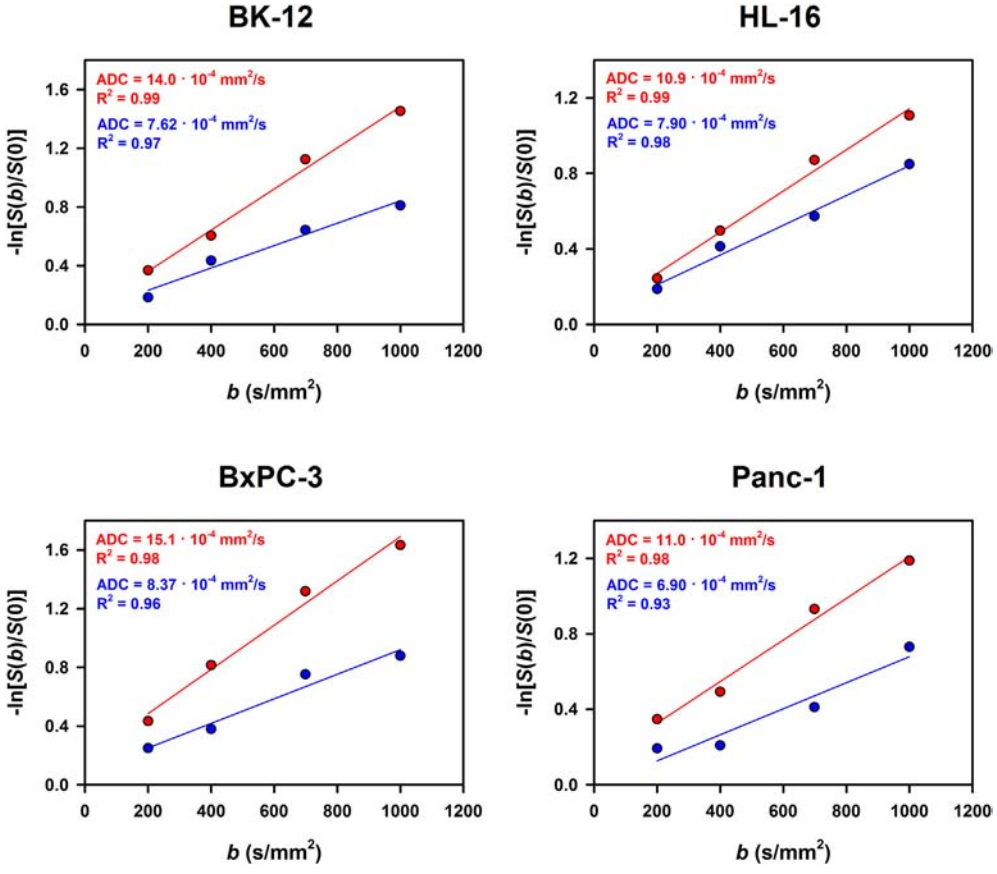

Figure 3. Monoexponential diffusion model. Representative plots of $-\ln[S(b)/S(0)]$ versus b (S, signal intensity; b, diffusion encoding constant) and the corresponding curve fits for single voxels of BK-12, HL-16, BxPC-3, and Panc-1 tumors. ADC was calculated from the slopes of the curves, and the data in each panel refer to two voxels, one with a low and the other with a high ADC value.

when the data complied with the conditions of normality and equal variance. Under other conditions, comparisons were carried out by nonparametric analysis using the Mann-Whitney rank-sum test (single comparisons). The Kolmogorov-Smirnov method and the Levene's method were used to verify normality and equal variance, respectively. Probability values of $P < .05$, determined from two-sided tests, were considered significant. The statistical analysis was carried out with SigmaStat statistical software.

Results

The tumors of the four models differed substantially in histological appearance (Figure 1). BK-12 tumors were moderately differentiated,

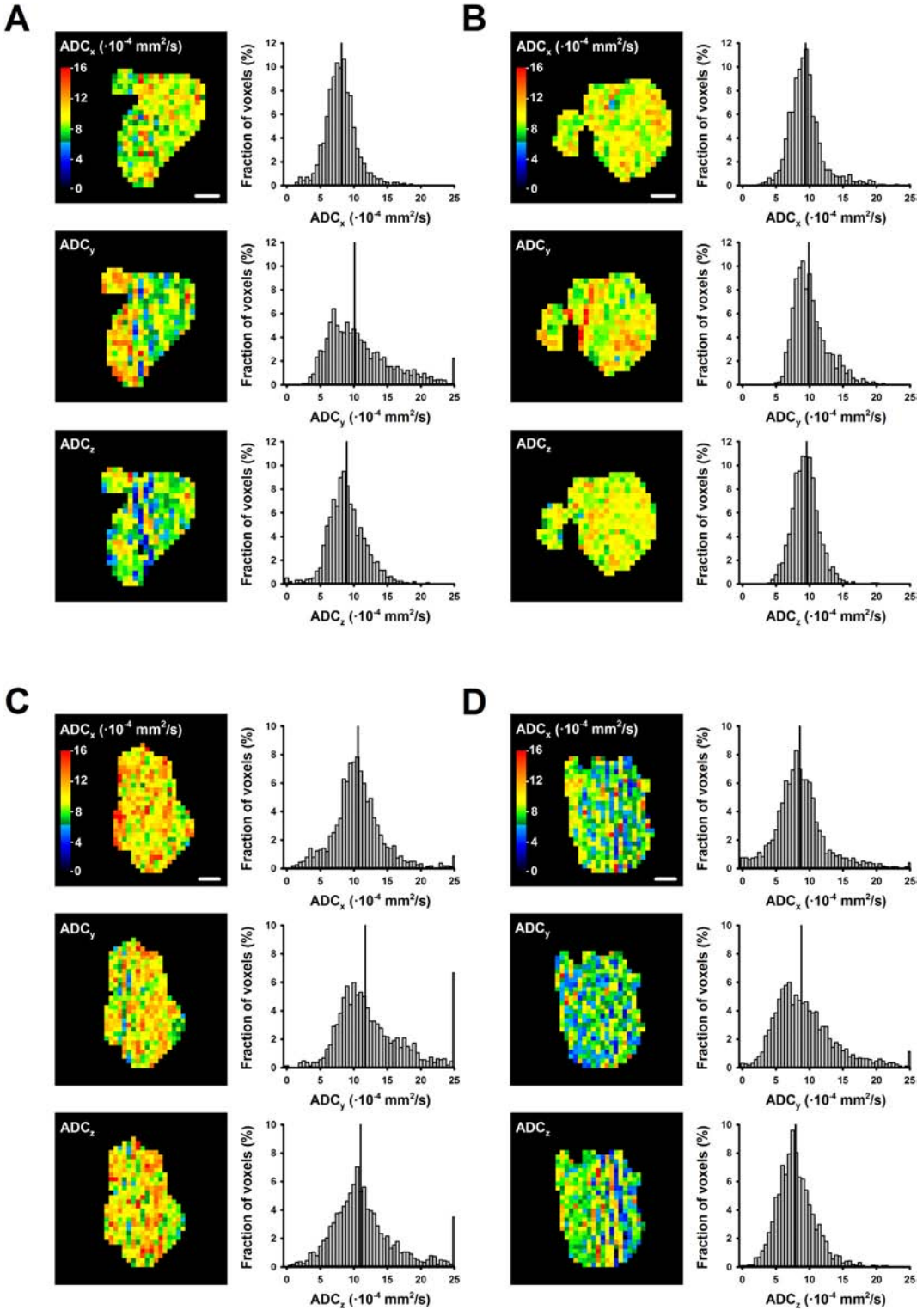

Figure 4. Directional ADC data. ADC maps and frequency distributions of a representative BK-12 (A), HL-16 (B), BxPC-3 (C), and Panc-1 (D) tumor recorded in the *X*, *Y*, and *Z* directions. The maps refer to a scan through the tumor center, whereas the frequency distributions refer to the entire tumor volume. Vertical line in the ADC frequency distributions, median value. Scale bars, 2.0 mm.

whereas HL-16 tumors were poorly differentiated, consistent with the donor patients' tumors. BxPC-3 tumors showed distinct ductal structures and were moderately differentiated, whereas Panc-1 tumors were nondifferentiated and showed an apparently random distribution of the tumor cells. Staining for CD31 revealed that blood vessels were located primarily in connective tissue in all tumor models, but HL-16 and Panc-1 tumors also showed some blood vessels in the tumor parenchyma. Staining for pimonidazole showed that the extent of hypoxia and the staining pattern differed among the tumor models. Hypoxia was seen primarily in central regions in BK-12 and BxPC-3 tumors, whereas HL-16 and Panc-1 tumors showed foci of hypoxic tissue scattered throughout the sections.

BK-12 and HL-16 tumors were treated with bevacizumab, and BxPC-3 and Panc-1 tumors were treated with sunitinib, and there were significant differences in microvascular density (MVD) and hypoxic fraction (HF_{Pim}) between treated and untreated tumors. By comparing treated and untreated tumors of approximately the same size (Figure 2*A*), it was revealed that AAT induced a decrease in MVD in BK-12 ($P < .001$), HL-16 ($P < .001$), and BxPC-3 ($P < .001$) tumors (Figure 2*B*) and an increase in HF_{Pim} in BK-12 ($P = .045$) and BxPC-3 ($P < .001$) tumors (Figure 2*C*). On the other hand, treated and untreated Panc-1 tumors did not differ significantly in MVD or HF_{Pim}.

DW-MRI was carried out with four diffusion encoding constants and diffusion gradient sensitization in three orthogonal directions. ADC was calculated by using a monoexponential diffusion model, and good fits to the acquired data were obtained for all three gradient directions, with correlation coefficients of $R^2 > 0.85$ (Figure 3). As expected for isotropic tumors, ADC was independent of the direction of the diffusion sensitization gradients (Figure 4).

Figure 5 depicts representative examples of nondirectional ADC maps and frequency distributions of untreated and treated tumors. In general, the ADC maps differed among the models, with the highest ADC values in BxPC-3 tumors and the lowest ADC values in Panc-1 tumors. The heterogeneity in ADC was substantial, both among tumors of the same model and within individual tumors, with high ADC values in peripheral as well as central tumor regions.

To investigate whether AAT-induced changes in MVD or HF_{Pim} can be detected by DW-MRI, tumors were given AAT or vehicle

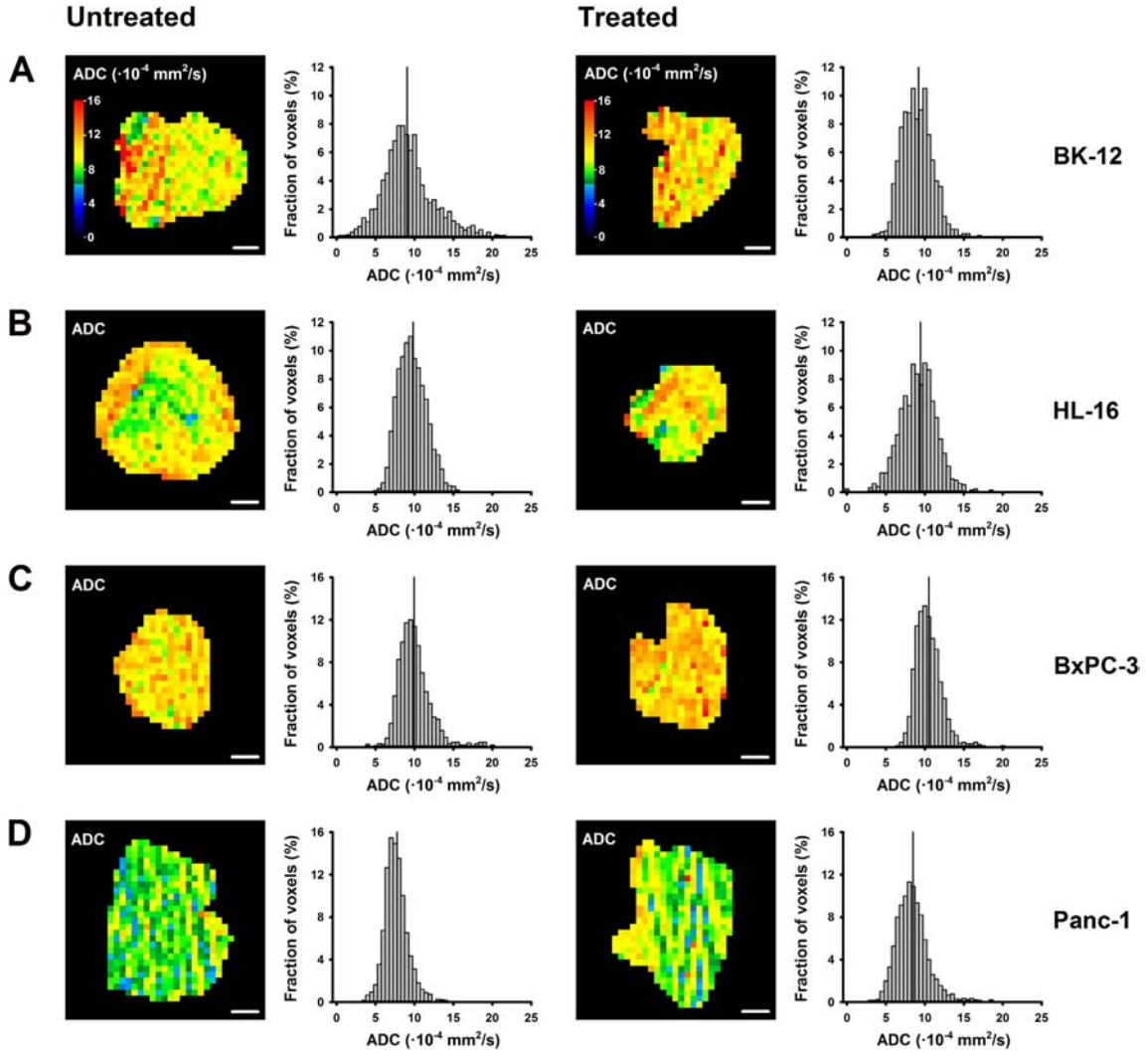

Figure 5. ADC data of untreated and treated tumors. Nondirectional ADC maps and frequency distributions of representative untreated and treated BK-12 (A), HL-16 (B), BxPC-3 (C), and Panc-1 (D) tumors. BK-12 and HL-16 tumors were treated with bevacizumab, and BxPC-3 and Panc-1 tumors were treated with sunitinib. The maps refer to a scan through the tumor center, whereas the frequency distributions refer to the entire tumor volume. Vertical line in the ADC frequency distributions, median value. Scale bars, 2.0 mm.

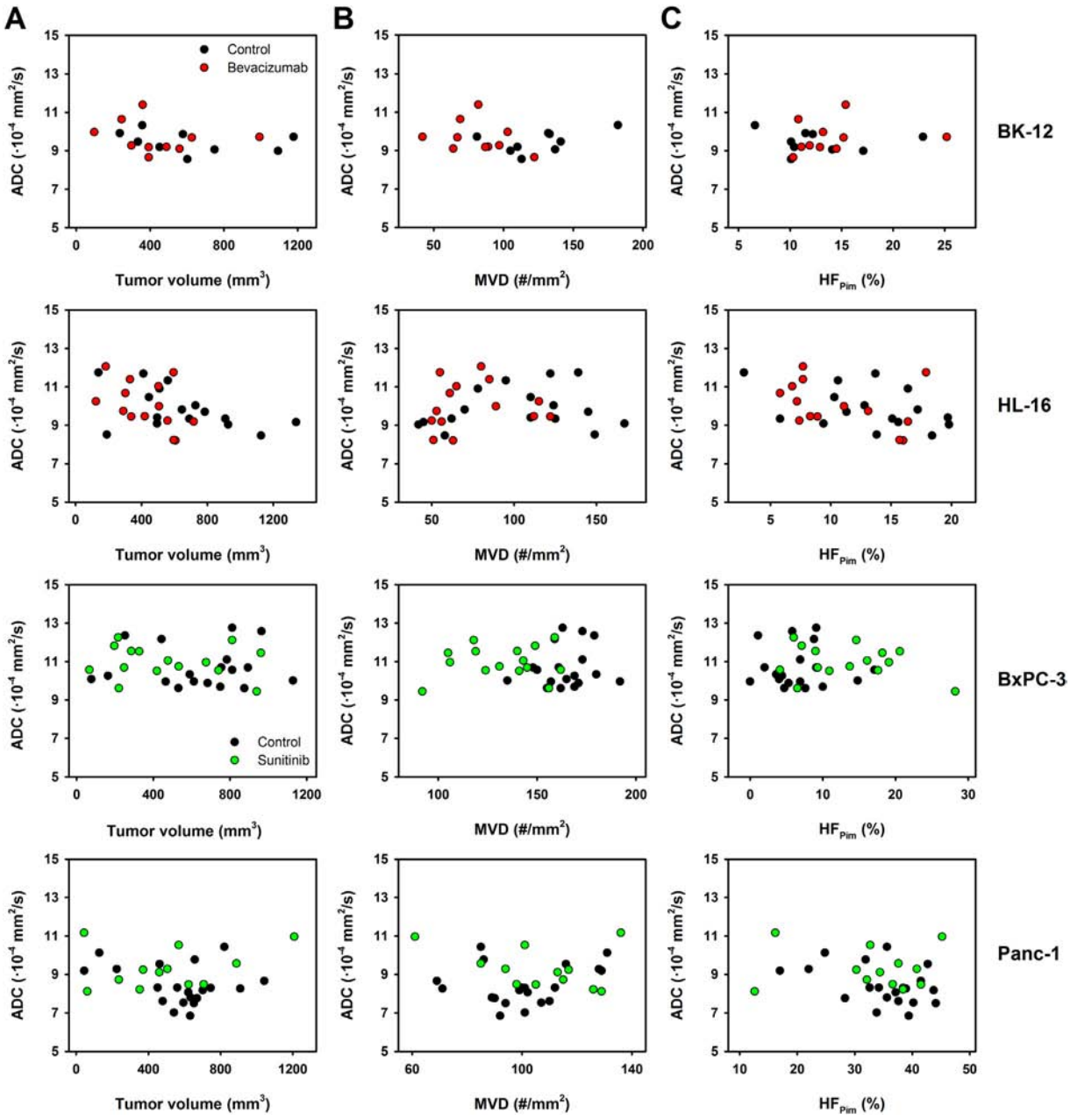

Figure 6. ADC, tumor volume, MVD, and HF_{Pim}. Median ADC versus tumor volume (A), MVD (B), and HF_{Pim} (C) for treated and untreated BK-12, HL-16, BxPC-3, and Panc-1 tumors. The BK-12 and HL-16 tumors were treated with bevacizumab, and the BxPC-3 and Panc-1 tumors were treated with sunitinib. Symbols, individual tumors.

treatment before being subjected to DW-MRI and histological examinations. Tumors differing considerably in volume were included in the study to ensure a wide range of MVD and HF_{Pim} values. Median ADC did not correlate with tumor volume (Figure 6*A*), MVD (Figure 6*B*), or HF_{Pim} (Figure 6*C*) in any of the tumor models, regardless of whether the tumors were treated or not ($P > .05$). Furthermore, median ADC differed among the tumor models ($P < .05$ for BxPC-3 versus BK-12, HL-16, and Panc-1; and Panc-1 versus BK-12 and HL-16) but not between treated and untreated tumors of the same model, with the only exception that median ADC was higher in treated than in untreated Panc-1 tumors (Figure 7). Because AAT had no effect on MVD or HF_{Pim} in Panc-1 tumors (Figure 2), the AAT-induced increase in median ADC was most likely due to microenvironmental changes other than changes in tumor vascularity and oxygenation. Taken together, the data presented in Figures 2, 6, and 7 demonstrate that DW-MRI is insensitive to intertumor heterogeneity in MVD and HF_{Pim} as well as AAT-induced changes in MVD and HF_{Pim}.

Discussion

Most experimental tumors show decreasing vascular density and increasing hypoxic fraction during growth [21]. In preclinical studies of antiangiogenic agents, it is of utmost importance to discriminate between treatment-induced and growth-induced changes in the tumor microenvironment. The study reported here was designed to facilitate this discrimination. It showed that ADC does not vary with tumor volume, MVD, or HF_{Pim} while confirming that ADC can differ significantly among tumor models. Moreover, our study

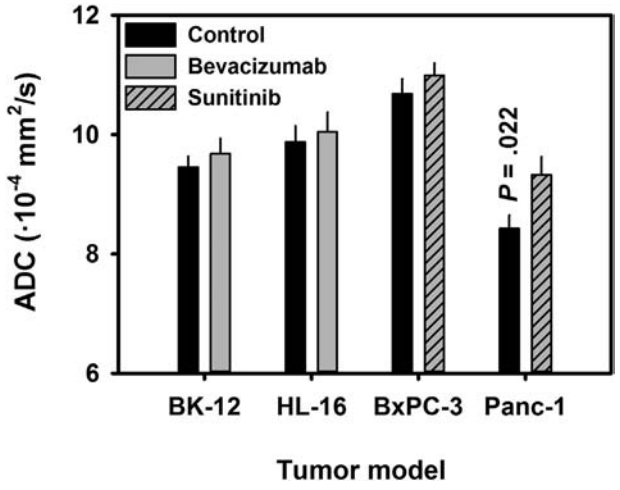

Figure 7. ADC data of untreated and treated tumors. The ADC of tumors treated with bevacizumab or sunitinib is compared with that of untreated control tumors. Columns and bars, mean of median ± standard error (n = 9-20).

revealed that untreated tumors and tumors given AAT can differ significantly in MVD and HF_{Pim} and that ADC maps are insensitive to these differences. Consequently, it is unlikely that DW-MRI can be used to monitor AAT-induced changes in the microenvironment of tumors.

Preclinical DW-MRI studies have significant advantages to clinical studies since the imaging conditions can be controlled more easily. In this study, the physiology of the imaged mice was monitored carefully, ensuring that the microenvironment of the tumor tissue was not perturbed during image acquisition. After imaging, it was verified that the tumors had not moved during the MRI, securing that reliable voxelwise ADC values could be calculated. Four diffusion encoding constants were used, and it was seen that a monoexponential diffusion model provided good fits to the data with high correlation coefficients and that the calculated ADC values were independent of the direction of the diffusion sensitization gradients.

The ADC of tumors depends on several properties of the imaged tissue [12,22], and it has been revealed that low ADC values can be a consequence of high cell density [23] or a collagen-rich extracellular matrix with a high density of protein fibers [16,24]. Tumors showing ductal structures may have high ADC values owing to little restriction to water diffusion within the ducts [16], and the ADC values of tumors with extensive necrotic regions are usually high because the membrane structures limiting the diffusion of water in viable tissue are broken down in tumor necroses [12,22,23]. In our study, AAT did not induce significant changes in the histological appearance of the tumor tissue, as revealed by comprehensive qualitative examinations of tumor cellularity, extracellular matrix, and ductal structures. Moreover, with the exception that a few minor necrotic foci could be detected in some BK-12 tumors, the tumors in this study did not show necrotic regions, and necroses were not induced by AAT, similar to what is seen in most human tumors treated with acceptable doses of antiangiogenic agents.

Some clinical investigations have suggested that tumors may show increased ADC after AAT [9,11,12,22]. Unfortunately, most of these investigations were not supported by histological examinations of the imaged tissue. However, when the histology was examined, the examination provided significant evidence that the increased ADC was caused by an AAT-induced increase in tumor necrosis. Studies of recurrent glioblastomas with severe necrotic regions have shown decreased ADC after AAT, and the decrease in ADC was attributed to decreased necrosis caused by treatment-induced vessel normalization and increased blood perfusion [25,26]. In a preclinical study of non-necrotic melanoma xenografts, it was shown that treatment with high doses of sunitinib induced necrotic regions and resulted in increased ADC [27], whereas treatment of the same melanoma model with moderate doses of bevacizumab did not induce necrosis and had no effect on ADC [17]. Thus, there is some evidence that the ADC of tumors may change after AAT, but the evidence is limited to treatments causing significant changes in tumor necrosis.

Our study suggests that adequate monitoring of AAT-induced changes in the microenvironment of tumors requires quantitative MRI strategies other than DW-MRI. There is some evidence that microvascular changes induced by AAT are detectable in parametric images provided by dynamic contrast-enhanced MRI, susceptibility contrast MRI, and intravoxel incoherent motion MRI [28–31]. Moreover, it has been suggested that AAT-induced changes in tumor oxygenation may be monitored by MRI methods using ultrasmall superparamagnetic iron oxide particles as contrast agents [32,33].

In summary, this study revealed that AAT with bevacizumab or sunitinib as antiangiogenic agent can induce significant changes in the MVD and HF_{Pim} of cervical and pancreatic carcinoma xenografts. The ADC maps of treated tumors did not differ from those of untreated tumors, and ADC was shown to be insensitive to intertumor heterogeneity in MVD and HF_{Pim}. Consequently, DW-MRI may not be a useful imaging modality for detecting changes in the microenvironment of tumors induced by AAT.

Acknowledgements

We thank Kanthi Galappathi for excellent technical assistance. We conducted the MRI at the MRI Core Facility for Preclinical Cancer Research, Oslo University Hospital.

References

[1] Abdollahi A and Folkman J (2010). Evading tumor evasion: current concepts and perspectives of anti-angiogenic cancer therapy. *Drug Resist Updat* **13**, 16–28.
[2] Gacche RN and Meshram RJ (2014). Angiogenic factors as potential drug target: efficacy and limitations of anti-angiogenic therapy. *Biochim Biophys Acta* **1846**, 161–179.
[3] Jayson GC, Hicklin DJ, and Ellis LM (2012). Antiangiogenic therapy—evolving view based on clinical trial results. *Nat Rev Clin Oncol* **9**, 297–303.
[4] Ebos JML and Kerbel RS (2011). Antiangiogenic therapy: impact on invasion, disease progression, and metastasis. *Nat Rev Clin Oncol* **8**, 210–221.
[5] Chen HX and Cleck JN (2009). Adverse effects of anticancer agents that target the VEGF pathway. *Nat Rev Clin Oncol* **6**, 465–477.
[6] Dhani N, Fyles A, Hedley D, and Milosevic M (2015). The clinical significance of hypoxia in human cancers. *Semin Nucl Med* **45**, 110–121.
[7] Jain RK (2013). Normalizing tumor microenvironment to treat cancer: bench to bedside to biomarkers. *J Clin Oncol* (17), 2205–2218.
[8] Martin JD, Fukumura D, Duda DG, Boucher Y, and Jain RK (2016). Reengineering the tumor microenvironment to alleviate hypoxia and overcome cancer heterogeneity. *Cold Spring Harb Perspect Med* **6**a027094.
[9] O'Connor JPB and Jayson GC (2012). Do imaging biomarkers relate to outcome in patients treated with VEGF inhibitors? *Clin Cancer Res* **18**, 6588–6598.
[10] Garcia-Figueiras R, Padhani AR, and Baleato-Gonzalez S (2016). Therapy monitoring with functional and molecular MR imaging. *Magn Reson Imaging Clin N Am* **24**, 261–288.
[11] Padhani AR (2011). Diffusion magnetic resonance imaging in cancer patient management. *Semin Radiat Oncol* **21**, 119–140.

[12] Yankeelov TE, Arlinghaus LR, Li X, and Gore JC (2011). The role of magnetic resonance imaging biomarkers in clinical trials of treatment response in cancer. *Semin Oncol* **38**, 16–25.

[13] Hurwitz H, Fehrenbacher L, Novotny W, Cartwright T, Hainsworth J, Berlin J, Baron A, Griffing S, and Holmgren E, et al (2004). Bevacizumab plus irinotecan, fluorouracil, and leucovorin for metastatic colorectal cancer. *N Engl J Med* **350**, 2335–2342.

[14] Roskoski Jr R (2007). Sunitinib: a VEGF and PDGF receptor protein kinase and angiogenesis inhibitor. *Biochem Biophys Res Commun* **356**, 323–328.

[15] Rofstad EK, Simonsen TG, Huang R, Andersen LM, Galappathi K, Ellingsen C, Wegner CS, Hauge A, and Gaustad JV (2016). Patient-derived xenograft models of squamous cell carcinoma of the uterine cervix. *Cancer Lett* **373**, 147–155.

[16] Wegner CS, Gaustad JV, Andersen LM, Simonsen TG, and Rofstad EK (2016). Diffusion-weighted and dynamic contrast-enhanced MRI of pancreatic adenocarcinoma xenografts: associations with tumor differentiation and collagen content. *J Transl Med* **14**, 161.

[17] Gaustad JV, Simonsen TG, Smistad R, Wegner CS, Andersen LM, and Rofstad EK (2015). Early effects of low dose bevacizumab treatment assessed by magnetic resonance imaging. *BMC Cancer* **15**, 900.

[18] Rofstad EK, Rasmussen H, Galappathi K, Mathiesen B, Nilsen K, and Graff BA (2002). Hypoxia promotes lymph node metastasis in human melanoma xenografts by up-regulating the urokinase-type plasminogen activator receptor. *Cancer Res* **62**, 1847–1853.

[19] Rofstad EK, Huang R, Galappathi K, Andersen LM, Wegner CS, Hauge A, Gaustad JV, and Simonsen TG (2016). Functional intratumoral lymphatics in patient-derived xenograft models of squamous cell carcinoma of the uterine cervix: implications for lymph node metastasis. *Oncotarget* **7**, 56986–56997.

[20] Rofstad EK, Galappathi K, Mathiesen B, and Ruud EB (2007). Fluctuating and diffusion-limited hypoxia in hypoxia-induced metastasis. *Clin Cancer Res* **13**, 1971–1978.

[21] Vaupel P, Thews O, Kelleher DK, and Hoeckel M (1998). Current status of knowledge and critical issues in tumor oxygenation. Results from 25 years research in tumor pathophysiology. *Adv Exp Med Biol* **454**, 591–602.

[22] Padhani AR, Liu G, Koh DM, Chenevert TL, Thoeny CS, Takahara T, Dzik-Jurasz A, Ross BD, Van Cauteren M, and Collins D, et al (2009). Diffusion-weighted magnetic resonance imaging as a cancer biomarker: consensus and recommendations. *Neoplasia* **11**, 102–125.

[23] Lyng H, Haraldseth O, and Rofstad EK (2000). Measurement of cell density and necrotic fraction in human melanoma xenografts by diffusion weighted magnetic resonance imaging. *Magn Reson Med* **43**, 828–836.

[24] Hompland T, Ellingsen C, Galappathi K, and Rofstad EK (2014). Connective tissue of cervical carcinoma xenografts: associations with tumor hypoxia and interstitial fluid pressure and its assessment by DCE-MRI and DW-MRI. *Acta Oncol* **53**, 6–15.

[25] Batchelor TT, Duda DG, di Tomaso E, Ancukiewicz M, Plotkin SR, Gerstner E, Eichler AF, Drappatz J, Hochberg FH, and Benner T, et al (2010). Phase II study of cediranib, an oral panvascular endothelial growth factor receptor tyrosine kinase inhibitor, in patients with recurrent glioblastoma. *J Clin Oncol* **28**, 2817–2823.

[26] Sorensen AG, Emblem KE, Polaskova P, Jennings D, Kim H, Ancukiewicz M, Wang M, Wen PY, Ivy P, and Batchelor TT, et al (2012). Increased survival of glioblastoma patients who respond to antiangiogenic therapy with elevated blood perfusion. *Cancer Res* **72**, 402–407.

[27] Gaustad JV, Pozdniakova V, Hompland T, Simonsen TG, and Rofstad EK (2013). Magnetic resonance imaging identifies early effects of sunitinib treatment in human melanoma xenografts. *J Exp Clin Cancer Res* **32**, 93.

[28] Hillman GG, Singh-Gupta V, Zhang H, Al-Bashir AK, Katkuri Y, Li M, Yunker CK, Patel AD, Abrams J, and Haacke EM (2009). Dynamic contrast-enhanced magnetic resonance imaging of vascular changes induced by sunitinib in papillary renal cell carcinoma xenograft tumors. *Neoplasia* **11**, 910–920.

[29] Boult JKR, Box G, Vinci M, Perryman L, Eccles SA, Jones C, and Robinson SP (2017). Evaluation of the response of intracranial xenografts to VEGF signaling inhibition using multiparametric MRI. *Neoplasia* **19**, 684–694.

[30] Shi C, Liu D, Xiao Z, Zhang D, Liu G, Liu G, Chen H, and Luo L (2017). Monitoring tumor response to antivascular therapy using non-contrast intravoxel incoherent motion diffusion-weighted MRI. *Cancer Res* **77**, 3491–3501.

[31] Robinson SP, Boult JKR, Vasudev NS, and Reynolds AR (2017). Monitoring the vascular response and resistance to sunitinib in renal cell carcinoma *in vivo* with susceptibility MRI. *Cancer Res* **77**, 4127–4134.

[32] Matsumoto S, Batra S, Saito K, Yasui H, Choudhuri R, Gadisetti C, Subramanian S, Devasahayam N, Munasinghe JP, and Mitchell JB, et al (2011). Antiangiogenic agent sunitinib transiently increases tumor oxygenation and suppresses cycling hypoxia. *Cancer Res* **71**, 6350–6359.

[33] Lemasson B, Christen T, Serduc R, Maisin C, Bouchet A, Le Duc G, Rémy C, and Barbier EL (2012). Evaluation of the relationship between MR estimates of blood oxygen saturation and hypoxia: effect of an antiangiogenic treatment on a gliosarcoma model. *Radiology* **265**, 743–752.